

xApp Conflict Mitigation with Scheduler

IDRIS CINEMRE¹ (*Member, IEEE*), TOKTAM MAHMOODI¹ (*Senior Member, IEEE*),
AMIRMOHAMMAD FARZANEH¹ (*Member, IEEE*)

¹Department of Engineering, Faculty of Natural, Mathematical & Engineering Sciences, King's College, London

CORRESPONDING AUTHOR: Idris Cinemre (e-mail: idris.1.cinemre@kcl.ac.uk).

ABSTRACT Open RAN (O-RAN) fosters multi-vendor interoperability and data-driven control but simultaneously introduces the challenge of coordinating pre-trained xApps that may produce conflicting actions. Although O-RAN specifications mandate offline training and validation to prevent the deployment of untrained or inadequately tested models, operational conflicts can still arise under dynamic and context-dependent conditions. This work proposes a scheduler-based conflict mitigation framework to address these challenges without requiring training xApps together or further xApp re-training. By examining an indirect conflict involving power and resource block allocation xApps and employing an Advantage Actor-Critic (A2C) approach to train both xApps and the scheduler, we illustrate that a straightforward A2C-based scheduler improves performance relative to independently deployed xApps and conflicting cases. Notably, among all tested deployment scenarios (including individual xApp deployment, multiple conflicting xApps, and limited scheduler configurations), augmenting the system with baseline xApps and enabling the scheduler to select from a broader pool achieves the highest total transmission rate, thereby underscoring the importance of adaptive scheduling mechanisms. These findings highlight the context-dependent nature of conflicts in automated network management, as two xApps may conflict under certain conditions but coexist under others. Consequently, the ability to dynamically update and adapt the scheduler to accommodate diverse operational intents is vital for future network deployments. By offering dynamic scheduling without re-training xApps, this framework advances practical conflict resolution solutions while supporting real-world scalability.

INDEX TERMS Open RAN (O-RAN), xApp, Conflict Resolution, Advantage Actor-Critic (A2C)

I. INTRODUCTION

The Radio Access Network (RAN)—a critical and costly component of cellular systems—is pivotal to 6G innovation [1] and shifting from monolithic and hardware-centric architectures to more agile and customizable frameworks [2]. The Open RAN (O-RAN) paradigm, widely regarded as a cornerstone of future 6G networks [3], accelerates this transition by disaggregating traditional RAN architectures and standardizing interfaces among key network functions, thereby increasing vendor flexibility while reducing deployment and maintenance costs [4]. By interconnecting virtualized components via open interfaces, O-RAN enables multi-vendor interoperability and data-driven closed-loop control, facilitating real-time monitoring and more sophisticated RAN interactions that culminate in flexible, cost-effective, and vendor-neutral network deployments.

Building upon the 3GPP functional disaggregation framework [5], which partitions the 5G gNB architecture into the Remote Unit (RU), Distributed Unit (DU), and Centralized Unit (CU)—termed O-RU, O-DU, and O-CU in O-RAN

nomenclature [6]—the O-RAN architecture delineates these distinct RAN entities (as illustrated in Fig. 1), thereby facilitating multi-vendor interoperability and flexible deployment of the functional components across different hardware infrastructures and network locations [7]. Specifically, O-DU, O-CU-CP, and O-CU-UP reside in the edge cloud to satisfy strict latency requirements while the O-RU is physically deployed in the cell site, with the alternative configurations of these functional units to accommodate various scenario requirements, as outlined in [8].

The O-RAN Alliance adopted the 7.2x functional split to reconcile the simplicity of the O-RU with the data rate and latency constraints at the O-RU/O-DU interface (i.e. Open Fronthaul (FH)) [9] and adopted split option 2 between the O-DU/O-CU [10], [11]. The O-CU manages higher-layer non-real-time processes (e.g., packet management) by serving as a logical node to host higher protocol layers—namely RRC, SDAP, and PDCP [12]. It is functionally divided into the control plane (O-CU-CP), which handles RRC procedures and the PDCP control segment, and the user

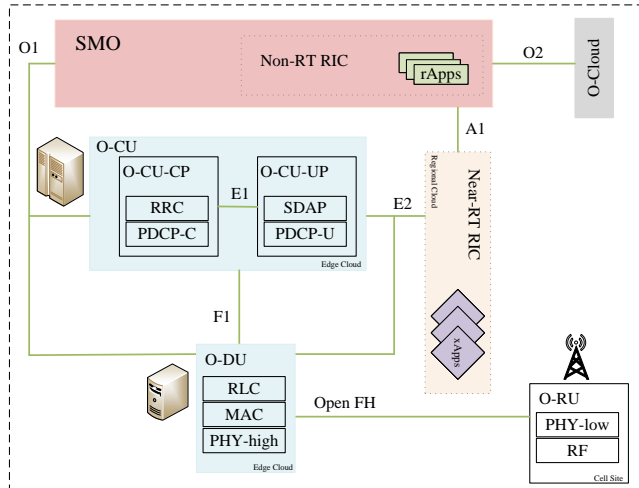


FIGURE 1: An overview of the O-RAN architecture

plane (O-CU-UP), which manages SDAP and the PDCP user segment. These components interact via the E1 interface, thereby enabling flexible scaling and reduced deployment costs for user-plane processing [4], [13]. The O-DU is also a logical node to oversee time-sensitive lower-layer operations and is responsible for hosting the lower-layer protocols of the RAN stack; specifically, the high PHY, MAC, and RLC layers—thereby executing baseband processing tasks such as scrambling, modulation, partial pre-coding, and physical resource block allocation [14], [15]. It manages multiple O-RUs over the open fronthaul and provides essential functionalities for data segmentation, scheduling, and multiplexing, with the MAC layer generating transport blocks for the physical layer based on data buffered at the RLC layer [9], [16]. This disaggregated design, controlled by the O-CU, enhances deployment flexibility, enables tighter synchronization of lower-layer operations, and allows for more efficient resource utilization. Finally, the O-RU is a physical node dedicated to low PHY layer and RF processing by performing time-domain operations—such as precoding, FFT/IFFT, and cyclic prefix addition/removal—the O-RU remains cost-effective to deploy and maintain at the cell site.

Within O-RAN, as given in Fig. 1, key entities called RAN Intelligent Controllers (RICs) host intelligent applications that dynamically and efficiently reconfigure the RAN. Specifically, third-party applications—rApps in the Non-Real-Time RIC (Non-RT RIC) and xApps in the Near-Real-Time RIC (Near-RT RIC)—operate independently of the underlying vendor to manage and optimize RAN functionalities under different latency requirements [9]. The Non-RT RIC, operating at time scales longer than 1s, complements the near-RT RIC’s intelligent RAN operation and optimization by offering guidance, enrichment information (EI), and AI/ML model management. Meanwhile, the Near-RT RIC, deployed at the network edge and operating control loops with periods ranging from 10ms to 1s, hosts xApps—each

a microservice specifically designed for radio resource management through specialized interfaces and service models. The Near-RT RIC can be deployed either at the edge or within the regional cloud [9], [17], whereas the Non-RT RIC is commonly hosted by the SMO, which manages the configuration and orchestration of RAN components [6], [14].

The E2 interface connects the Near-RT RIC to RAN nodes for near-real-time monitoring and control loops, while the A1 interface links the Near-RT RIC with the Non-RT RIC to enable policy-based management and facilitate the transfer of EI. Additionally, the O1 interface ensures overarching management and orchestration of O-RAN components, supporting advanced control and automation [18]. In addition, the O-CU terminates the E2 interface to link with the Near-RT RIC and uses the O1 interface for integration with the SMO framework [19], enabling advanced control, data-driven optimization, and automation. Meanwhile, the O-DU terminates multiple interfaces, including E2, F1, and open FH, and connects to the SMO via O1 [19]. Moreover, the O2 interface connects the SMO to the O-Cloud, a cloud computing platform that hosts O-RAN functions such as the Near-RT RIC, O-CU-CP, O-CU-UP, and O-DU [20], facilitating the management of both O-Cloud infrastructure and associated workloads [16], [21].

xApps are third-party pluggable modules that extend RAN capabilities [2] by implementing specialized, advanced algorithms for radio resource management [22]–[24], slicing [25], interference mitigation [26], [27], and mobility optimization [28]–[30]. Leveraging the standardized E2 interface, xApps can subscribe to performance metrics or event indications and issue corresponding policy-based control directives to the RAN. The Near-RT RIC mediates these interactions, enabling a closed-loop control mechanism in which xApps continuously analyze incoming data and dynamically optimize network behavior (e.g., by adjusting resource allocations or triggering handovers). According to O-RAN specifications [31], untrained xApps are not permitted; each model must undergo offline training and validation before publication in an AI/ML catalog, thereby mitigating outages or inefficiencies caused by underperforming models. Nonetheless, the concurrent operation of multiple trained xApps can introduce conflicts in network operations, as detailed in the subsequent section.

II. BACKGROUND

The potential conflict types among xApps were introduced under the Near-RT RIC architecture [32]. Recently, the O-RAN Alliance’s Working Group 3 (WG3) published an independent technical specification on conflict mitigation [33], analyzing these conflict types and detailing the methods for conflict detection, resolution, and avoidance. This functionality is critical, as multiple xApps—each pursuing distinct objectives—can produce conflicting actions when deployed concurrently. According to O-RAN technical specifications

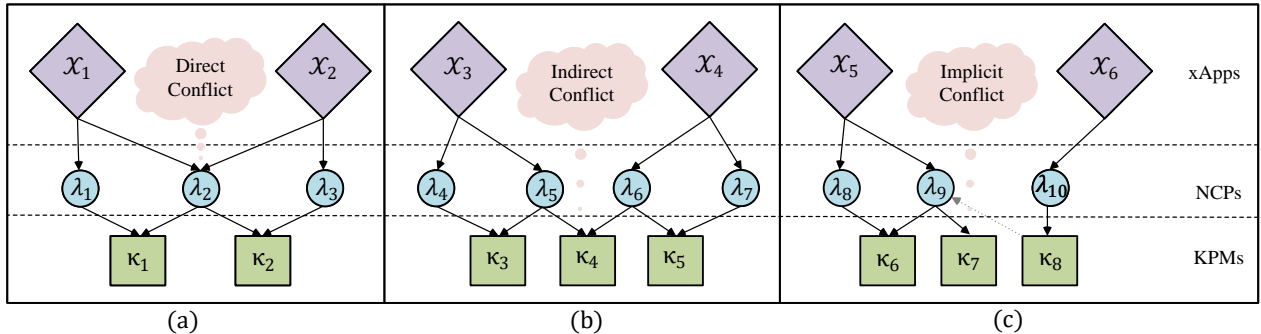


FIGURE 2: Conflict Types

in [33], these conflicts among xApps (i.e. $\mathcal{X}_1, \mathcal{X}_2, \dots$) are categorized as follows:

- *Direct conflict*: Occurs when multiple xApps request incompatible adjustments to the same configuration of one or more shared network control parameters (NCPs) (i.e. $\lambda_1, \lambda_2, \dots$) within the O-RAN. As illustrated in Fig. 2(a), if two xApps, \mathcal{X}_1 and \mathcal{X}_2 , attempt to modify the same NCP, λ_2 , in opposite directions or with inconsistent magnitudes, a conflict ensues. For example, \mathcal{X}_1 may increase transmission power to reduce cell-edge outage, while \mathcal{X}_2 may decrease it to mitigate inter-cell interference and enhance capacity. Similarly, \mathcal{X}_1 may raise antenna tilt to expand coverage, whereas \mathcal{X}_2 may lower tilt to confine signal propagation and reduce interference.
- *Indirect conflict*: Arises when multiple xApps modify different NCPs to optimize the same key performance metrics (KPMs) (i.e. $\mathcal{K}_1, \mathcal{K}_2, \dots$), thereby introducing unintentional interference with each other's objectives. As illustrated in Fig. 2(b), \mathcal{X}_3 adjusts (λ_4, λ_5) while \mathcal{X}_4 adjusts (λ_6, λ_7) — yet both aim to optimize the same KPM, \mathcal{K}_4 , in opposite directions or with inconsistent target values. For instance, \mathcal{X}_3 might adjust the cell individual offset to balance cell load, while \mathcal{X}_4 modifies the cell's electrical tilt to enhance capacity—both altering the effective cell boundary and thus creating an indirect conflict on the same KPM [34].
- *Implicit conflict*: Appears when multiple xApps independently optimize distinct KPMs by tuning different NCPs, yet inadvertently impact each other's objectives. These conflicts often remain hidden because the interdependence between the xApps is not immediately evident. As illustrated in Fig. 2(c), \mathcal{X}_5 tunes (λ_8, λ_9) while \mathcal{X}_6 modifies (λ_{10}) , each pursuing distinct KPMs. However, \mathcal{K}_8 influences one of \mathcal{X}_5 's NCPs, thereby implicitly affecting \mathcal{K}_7 . For example, an Energy Efficiency (EE) xApp may aim to minimize overall power consumption by deactivating certain RUs, while a Slice Management (SM) xApp simultaneously strives to meet high resource demands for bandwidth-intensive applications. These competing goals—reducing energy

usage vs. maximizing throughput—generate an implicit conflict [35].

Existing research on conflict detection and resolution in O-RAN has explored a range of strategies, generally falling into two main categories: *prioritization* and *pre-training*. In [35], a conflict mitigation (CM) component is introduced within the Near-RT RIC, comprising conflict detection (CD) and conflict resolution (CR) modules. The system leverages manually configured or dynamically learned parameter groups (PGs) to track parameter interactions affecting the same network area. The CD module flags indirect conflicts by comparing newly received E2 control messages against previously allowed configurations in each PG, and the CR module resolves conflicts by prioritizing one xApp's configuration while rejecting others. Although conceptually straightforward, this approach exhibits limitations, including a simplistic resolution mechanism, potentially cumbersome PG configuration, and the requirement for KPM estimation prior to xApp selection under all conditions. Its extension in [34] subdivides the CD module into three specialized submodules, each addressing a distinct conflict type, and provides further guidance on detecting direct and implicit conflicts.

The study, named as COMIX, outlined in [36] employs a similar conflict detection procedure by defining parameter groups and capturing KPM interactions. As part of the conflict resolution method, each action proposed by the pre-trained xApps is assessed through a scoring function, such as fairness, maximum throughput, or minimum power, using a network digital twin (NDT). However, requiring the NDT to evaluate both actions, and testing every xApp-generated value of NCPs in this manner, could pose significant latency challenges and call into question the necessity of relying on pre-trained xApps. Additionally, the success of the conflict resolution strategy hinges heavily on the performance of the NDT.

A more comprehensive conflict-management solution is provided by the PACIFISTA framework in [37], operating within the SMO environment. By interfacing with RICs and RAN nodes to collect profiling data, PACIFISTA dynamically deploys, monitors, and removes xApps/rApps based

on predefined conflict-management policies. Unlike earlier methods, it thoroughly evaluates the severity and potential impact of conflicts through statistical analysis of control parameters and KPMs under varied operational conditions (e.g., UE density, signal quality, traffic load). When the severity indexes computed by Kolmogorov-Smirnov, Integral Area, and Chi-Square tests exceed a specified threshold, PACIFISTA either blocks or removes offending applications, thereby prioritizing those that optimize network performance. The principal challenge lies in constructing detailed statistical profiles for each application across multiple operational scenarios and multi-application interactions.

The QoS-Aware Conflict Mitigation (QACM) method proposed in [38] addresses conflicts by minimizing the weighted distances of xApp utilities from their QoS thresholds and the squared sum of QoS satisfaction indicators. Deployed as the conflict mitigation controller (CMC) within the CM framework proposed in [35], QACM expands on Nash’s Social Welfare Function and Eisenberg-Gale solutions [39] by incorporating explicit QoS thresholds into its optimization. This design ensures that most xApps meet their QoS requirements, yielding superior performance relative to baseline schemes in both priority and non-priority scenarios. However, the approach assumes reliable KPM prediction which can be challenging in the dynamic nature of RAN conditions where NCPs and dynamic conditions substantially influence KPM behaviors.

Team learning-based methods provide another avenue for conflict mitigation, as demonstrated in [40], where a deep Q-network (DQN) trains xApps collectively to foster cooperation and eliminate conflicts. While effective, this approach presupposes that all xApps can be jointly trained, which may be infeasible when they originate from different vendors. Building on this idea, the team multi-agent deep reinforcement learning (TMADRL) framework in [41] extends DQN-based training to multiple xApps controlling different RAN parameters, showing superior performance over sequential and concurrent baselines of MADRL in terms of energy utilization and throughput. However, the method requires careful selection of xApps with a common goal, joint pre-training with cooperative strategies, and significant overhead for action exchange, a challenge that escalates as the number of xApps grows.

The conflict-mitigation technique termed xApp distillation is proposed in [42], consolidating multiple ML-based xApps into a single DQN-based controller. Unlike conventional O-RAN conflict mitigation, which discards actions from some xApps, the proposed method also aggregates the experience of all xApps by distilling their policies into a single DQN-based xApp. This student network thus learns a more comprehensive policy from multiple teacher xApps, each of which was pre-trained to manage different or overlapping RAN parameters. The effectiveness of the method depends on teacher quality, and substantial offline data collection for various conditions. Moreover, deploying a single dis-

tilled model may limit operational flexibility and require re-distillation if network conditions evolve.

Unless an accurate digital twin of the network is available, it is impractical to assume that KPMs can be accurately estimated for every scenario involving diverse combinations of active xApps. Moreover, given that all xApps have been trained, tested, and verified, they cannot be modified further [9], [31]. In practical conflict management scenarios, it is essential to recognize that conflicts are often context-dependent (i.e. operational conditions), meaning that two applications may conflict in certain circumstances but coexist in others. Moreover, predicting which applications will be active concurrently is inherently difficult, making it unlikely that those trained together will ultimately operate together in real-world deployments.

This study introduces a framework that incorporates a scheduler for selecting active xApps based on context variables and a specified KPM, without requiring xApp re-training. It has been shown that independently deployed xApps can lead to conflicts, which are also shown to be highly context-dependent. To address this, an intent-driven, scheduler-based conflict mitigation framework is defined, exemplified by a simulation scenario of indirect conflict involving Power and RGB allocation xApps. The Advantage Actor-Critic (A2C) method is employed to train both the xApps and the scheduler, with two distinct scheduling approaches determining which xApps are activated according to contextual variables and the target KPM specified in the user intent.

The paper is organized as follows: In Section III, the system model is presented, including a summary spanning from the REINFORCE algorithm to A2C methods, and the modeling of power and RGB allocation xApps using A2C. In Section IV, the proposed scheduler management framework with associated RIC components is introduced. Subsequently, Section V provides the training results of the xApps, the proposed methods for scheduler design, and simulation results. Finally, conclusions are drawn in Section VI.

III. SYSTEM MODEL

This study considers an O-RAN cellular network architecture with B O-RUs concurrently serving U users, managed through the RICs within the O-RAN framework. In this setting, a minimum of $n \geq 2$ distinct xApps, denoted as $\{\mathcal{X}_1, \mathcal{X}_2, \dots, \mathcal{X}_n\}$, are deployed within the Near-RT RIC to control KPMs in a downlink OFDM scenario. In this model, it is assumed that each O-RU has R available resource block groups (RBGs), bundles of consecutive resource blocks as defined in [43], representing the smallest time-frequency resource to allocate users.

At any time step $t \in \{1, 2, \dots, \tilde{t}\}$ within episode e , $\delta_{t,e}^{b,r,u}$ is a binary variable that indicates whether O-RU $b \in B$ allocates RBG $r \in R$ to user $u \in U$, where $\delta_{t,e}^{b,r,u} \in \{0, 1\}$, $\forall b, r, u$ and $\sum_{u \in U} \delta_{t,e}^{b,r,u} = 1$, $\forall b, r$. The

instantaneous traffic arrivals for each RBG r allocated to user u at time step t in episode e , denoted by $\varrho_{t,e}^{b,r,u}$, are assumed to follow a Poisson distribution with mean data arrival rate d_e , which remains constant throughout the episode.

Let $p_{t,e}^{b,r,u}$ denote the power allocated on RBG r at O-RU b for user u during time slot t in episode e . In a discrete-power setting, each $p_{t,e}^{b,r,u}$ takes values from a finite set of feasible power levels, $p_{t,e}^{b,r,u} \in \mathcal{P}$ where $\mathcal{P} \subseteq [P_{\min}, P_{\max}]$. Following the quantization-based discretization in [44], [45], the set of feasible power levels, \mathcal{P} , is given as

$$\mathcal{P} = \{0\} \cup \left\{ P_{\min} \beta^k : k = 0, 1, \dots, K-2 \right\}, \quad (1)$$

where

$$\beta = \left(\frac{P_{\max}}{P_{\min}} \right)^{\frac{1}{K-2}}, \quad (2)$$

and K represents the total number of quantization levels, including the 0 level to indicate no transmission on the allocated RBG. Additionally, the system incorporates user mobility, where each user u moves at a constant random speed $v_e^u \in (V_{\min}, V_{\max})$ with a defined $\mathbb{E}[v_e^u]$ throughout episode e , and has a specified probability ρ of altering direction $\Theta_{t,e}^u$ in each time slot t . At any given time slot t in episode e , the position of user u , denoted by $(x_{t,e}^u, y_{t,e}^u)$, is updated as:

$$x_{t+1,e}^u = x_{t,e}^u + v_e^u \cos(\Theta_{t,e}^u), \quad y_{t+1,e}^u = y_{t,e}^u + v_e^u \sin(\Theta_{t,e}^u). \quad (3)$$

The direction at time $t+1$ is given episode e as

$$\Theta_{t+1,e}^u = \begin{cases} \Theta_{t,e}^u, & \text{with probability } (1-\rho) \\ \Theta_{t,e}^u + \Delta\Theta, & \text{with probability } \rho \end{cases} \quad (4)$$

where $\Delta\Theta \in [0, 2\pi]$ denotes the change in direction and initial direction of each user at the start of episode e , $\Theta_{0,e}^u$, is drawn from a uniform distribution over the interval $[0, 2\pi]$ (i.e. $\Theta_{0,e}^u \sim \mathcal{U}(0, 2\pi)$). This ensures that all possible initial headings are equally likely.

The logarithmic normalized channel state information (CSI) of user u for allocated RBG r from O-RU b , denoted by $\zeta_{t,e}^{b,r,u}$, is defined as

$$\zeta_{t,e}^{b,r,u} = \left\{ \log_2 \left(1 + \frac{\sum_{u \in U} \delta_{t,e}^{b',r,u} h_{t,e}^{b',u}}{\sum_{u \in U} \delta_{t,e}^{b,r,u} h_{t,e}^{b,u}} \right) \middle| b' \in B, b' \neq b \right\}, \quad (5)$$

where $h_{t,e}^{b,u}$ denotes the channel coefficient between O-RU b and user u in the position of $(x_{t,e}^u, y_{t,e}^u)$ and the numerator accounts for interference from all other O-RUs, $b' \neq b$. Similarly, the signal-to-interference-plus-noise ratio (SINR) for the link between O-RU b and user u on RBG r at time t in episode e is

$$\xi_{t,e}^{b,r,u} = \frac{\delta_{t,e}^{b,r,u} h_{t,e}^{b,u} p_{t,e}^{b,r}}{\sum_{b' \in B, b' \neq b} \sum_{u' \in U^{b'}} \delta_{t,e}^{b',r,u'} h_{t,e}^{b',u'} p_{t,e}^{b',r} + \sigma^2}, \quad (6)$$

where σ^2 is the noise power. Then, the transmission capacity of RBG r allocated by O-RU b to user u can be formulated as

$$C_{t,e}^{b,r,u} = \mathcal{B}^r \log_2 \left(1 + \xi_{t,e}^{b,r,u} \right), \quad (7)$$

where \mathcal{B}^r denotes the bandwidth of RBG r . The transmission rate $\Psi_{t,e}^{b,r,u}$ equals to $C_{t,e}^{b,r,u}$ if the length of the queued data exceeds the transmission capacity within a time slot, in which case any data beyond that capacity is assumed to be discarded. Otherwise, (i.e. $C_{t,e}^{b,r,u} T \geq \sum_{u \in U} \delta_{t,e}^{b,r,u} \varrho_{t,e}^{b,r,u}$), and the transmission rate is given by $\Psi_{t,e}^{b,r,u} = \varrho_{t,e}^{b,r,u} / T$, where T represents the duration of the time slot t .

A. From REINFORCE to Advantage Actor-Critic (A2C)

The REINFORCE algorithm [46] is a foundational policy-based method in reinforcement learning (RL) that optimizes the expected return by adjusting the policy parameters in the direction of the policy gradient. Formally, the gradient of the expected return with respect to θ is:

$$\nabla_{\theta} J(\theta) = \mathbb{E}_{\pi} [\nabla_{\theta} \log \pi_{\theta}(\mathbf{a}_t | \mathbf{s}_t) G_t], \quad (8)$$

where $\pi_{\theta}(\mathbf{a}_t | \mathbf{s}_t)$ is the probability of taking action \mathbf{a}_t in state \mathbf{s}_t and $G_t = \sum_{j=t}^{\tilde{t}-1} \gamma^{j-t} r_j$ denotes the return with γ is the discount factor and reward r following time step t . This leads to update the policy parameters θ via

$$\theta \leftarrow \theta + \eta \sum_{t=0}^{\tilde{t}-1} \gamma^t G_t \nabla_{\theta} \log \pi_{\theta}(\mathbf{a}_t | \mathbf{s}_t), \quad (9)$$

where η is learning rate. While this Monte Carlo approach is conceptually straightforward, it exhibits high variance and necessitates waiting until an episode terminates [47]. A common variance reduction technique is to subtract a state-dependent baseline $b(\mathbf{s}_t)$ [48], which does not depend on the chosen action a_t , leading to the unbiased gradient

$$\nabla_{\theta} J(\theta) \approx \sum_t \nabla_{\theta} \log \pi_{\theta}(\mathbf{a}_t | \mathbf{s}_t) (G_t - b(\mathbf{s}_t)). \quad (10)$$

Selecting $b(\mathbf{s}_t) = V^{\pi}(\mathbf{s}_t)$, the state-value function, gives rise to the *Actor-Critic* framework [49], [50]. In particular, $V^{\pi}(\mathbf{s}_t)$ is approximated by a learnable critic $V_{\phi}(\mathbf{s}_t)$, and one minimizes the mean squared error $(G_t - V_{\phi}(\mathbf{s}_t))^2$ to train ϕ , while the policy gradient (actor update) becomes

$$\nabla_{\theta} J(\theta) \approx \sum_t \nabla_{\theta} \log \pi_{\theta}(\mathbf{a}_t | \mathbf{s}_t) (G_t - V_{\phi}(\mathbf{s}_t)). \quad (11)$$

Replacing the full return G_t with the one-step return $G_{t:t+1} = r_t + \gamma V_{\phi}(\mathbf{s}_{t+1})$ further decreases variance by bootstrapping from the critic's estimate. This yields the *advantage*,

$$A_t = r_t + \gamma V_{\phi}(\mathbf{s}_{t+1}) - V_{\phi}(\mathbf{s}_t), \quad (12)$$

as capturing how much better (or worse) the action \mathbf{a}_t is compared to the critic's baseline $V_{\phi}(\mathbf{s}_t)$ so that the policy gradient takes the form

$$\nabla_{\theta} J(\theta) \approx \sum_t \nabla_{\theta} \log \pi_{\theta}(\mathbf{a}_t | \mathbf{s}_t) A_t, \quad (13)$$

commonly referred to as *Advantage Actor-Critic (A2C)*. The REINFORCE update in (9) thus becomes

$$\theta \leftarrow \theta + \eta \sum_{t=0}^{\tilde{t}-1} \gamma^t [G_{t:t+1} - V_{\phi}(\mathbf{s}_t)] \nabla_{\theta} \log \pi_{\theta}(\mathbf{a}_t | \mathbf{s}_t). \quad (14)$$

In A2C approach, a synchronous variant of the Asynchronous Advantage Actor-Critic (A3C) algorithm introduced in [51], a policy network (the *Actor*), $\pi_\theta(\mathbf{a}_t | \mathbf{s}_t)$, outputs a probability distribution over actions \mathbf{a}_t given state \mathbf{s}_t while a value network (the *Critic*), V_ϕ , estimates the expected return from state \mathbf{s}_t , $V_\phi(\mathbf{s}_t) \approx \mathbb{E}[G_t | \mathbf{s}_t]$. The *advantage function*, $A(\mathbf{s}_t, \mathbf{a}_t) = G_{t:t+1} - V_\phi(\mathbf{s}_t)$, compares the discounted one-step return $G_{t:t+1}$ to the Critic's baseline $V_\phi(\mathbf{s}_t)$. By quantifying how much better (or worse) a particular action is relative to the baseline, this formulation reduces the variance of policy gradient updates while maintaining low bias, thereby enhancing learning stability. The policy gradient update to θ aims to maximize the expected advantage

$$\sum_{t=0}^{\tilde{t}-1} A_t \log \pi_\theta(\mathbf{a}_t | \mathbf{s}_t), \quad (15)$$

while the critic update seeks to minimize

$$\sum_{t=0}^{\tilde{t}-1} (G_t - V_\phi(\mathbf{s}_t))^2, \quad (16)$$

leading to a combined loss function:

$$\mathcal{L}(\theta, \phi) = - \sum_{t=0}^{\tilde{t}-1} [A_t \log \pi_\theta(\mathbf{a}_t | \mathbf{s}_t)] + \alpha \sum_{t=0}^{\tilde{t}-1} (G_t - V_\phi(\mathbf{s}_t))^2 \quad (17)$$

where $\alpha > 0$ controls the balance between policy and value losses.

B. Power and RGB Allocation xApps with A2C

The power allocation in multi-cell networks has been extensively investigated in the literature using various RL-based methods, including DQN [45], [52], [53], DDQN [54], A2C [55], A3C [44], TD3 [56], and DDPG [57]. The DQN-based power allocation xApp defined in [40] is re-designed with A2C method to allocate the optimal power level to each RBG across all O-RUs by defining input states at time t within episode e as

$$\mathbf{s}_{t,e} = \left[\zeta_{t,e}^{b,r,u}, \Psi_{t,e}^{b,r,u}, p_{t,e}^{b,r,u}, \varrho_{t,e}^{b,r,u} \right]_{b \in B, r \in R, u \in U} \quad (18)$$

where $\mathbf{s}_{t,e}$ contains four features for every RBGs of each O-RU assigned to the users. The action vector, representing the power allocations for all RBGs, is given by:

$$\mathbf{a}_{t,e} = \left[p_{t+1,e}^{b,r,u} \right]_{b \in B, r \in R, u \in U} \quad (19)$$

where each element of $\mathbf{a}_{t,e}$ is drawn from a finite set \mathcal{P} defined in (1).

In A2C approach, a policy network (the *Actor*), π_θ , outputs a probability distribution over possible power levels for each RBG per O-RU, while a value network (the *Critic*), V_ϕ , estimates the expected return for a given state. The joint policy of independent action selection per RBG, a^r ,

$$\pi_\theta(\mathbf{a}_{t,e} | \mathbf{s}_{t,e}) = \prod_{(b,r,u)} \pi_\theta(a_{t,e}^r = p_{t+1,e}^{b,r,u} | \mathbf{s}_{t,e}). \quad (20)$$

where the categorical distribution over the K power levels for each RBG r is defined as

$$\pi_\theta(a^r | \mathbf{s}_{t,e}) = \frac{\exp(z_{r,a^r}(\mathbf{s}_{t,e}))}{\sum_{\iota=0}^{K-1} \exp(z_{r,\iota}(\mathbf{s}_{t,e}))}, \quad (21)$$

where $a^r \in \mathcal{P}$ and $z_{r,\iota}(\mathbf{s}_{t,e})$ is the logit for the ι -th power level at the r -th RBG.

The critic, $V_\phi(\mathbf{s}_{t,e})$, is a scalar-valued neural network that approximates $\mathbb{E}[G_{t,e} | \mathbf{s}_{t,e}]$, where the discounted return at time step t is

$$G_{t,e} = \sum_{j=0}^{\tilde{t}-t-1} \gamma^j \tau_{t+j,e}, \quad \gamma \in (0, 1). \quad (22)$$

Here, \tilde{t} is the final timestep within an episode, e , and τ_{t+j} is the reward at time $t+j$.

Resource allocation in O-RAN has been examined from the perspective of physical resource blocks using a variety of methods; random forest classifier [58], probabilistic forecasting techniques [59], DRL [60], A2C [61], DQN [24]. In this work, the DQN-based radio resource allocation xApp presented in [40] is re-designed as an RGB allocation xApp, wherein the A2C method is employed to assign RBGs to users across O-RUs. This procedure parallels that of the power allocation xApp, wherein an *Actor* network outputs a probability distribution over RBG assignment decisions

$$\pi_\theta(\mathbf{a}_{t,e} | \mathbf{s}_{t,e}) = \prod_{(b,r,u)} \pi_\theta(a_{t,e}^r = \delta_{t+1,e}^{b,r,u} | \mathbf{s}_{t,e}) \quad (23)$$

where the state $\mathbf{s}_{t,e}$ and actions $\mathbf{a}_{t,e}$ are defined as

$$\mathbf{s}_{t,e} = \left[\delta_{t,e}^{b,r,u} \Gamma_t^{b,r,u}, \delta_{t,e}^{b,r,u} R_t^{b,r,u}, \delta_{t,e}^{b,r,u} p_t^{b,r,u}, \delta_{t,e}^{b,r,u} L_t^{b,r,u} \right]_{b \in B, r \in R, u \in U}$$

$$\mathbf{a}_{t,e} = \left[\delta_{t+1,e}^{b,r,u} \right]_{b \in B, r \in R, u \in U}, \quad \delta_{t+1,e}^{b,r,u} \in \{0, 1\}. \quad (24)$$

At each time step t , the xApp determines the allocation of RBGs to users for the next time step $t+1$. Each element $\delta_{t+1,e}^{b,r,u}$ indicates whether O-RU b assigns RBG r to user u at the next time step $t+1$. *Critic* network estimates the expected return from a given state, $\mathbf{s}_{t,e}$, $V_\phi(\mathbf{s}_{t,e}) \approx \mathbb{E}[G_{t,e} | \mathbf{s}_{t,e}]$.

IV. SCHEDULER DRIVEN xAPP MANAGEMENT FRAMEWORK

This study proposes a scheduler within the Near-RT RIC whose primary objective is to coordinate the xApps deployed by the Non-RT RIC in accordance with the intents provided by the MNO, as illustrated in Fig. 3.

A. SMO and Non-RT RIC

The Non-RT RIC facilitates a flexible architecture by offering two primary services [31]: intent-based network management (IBNM) and intelligent orchestration (IO). IBNM

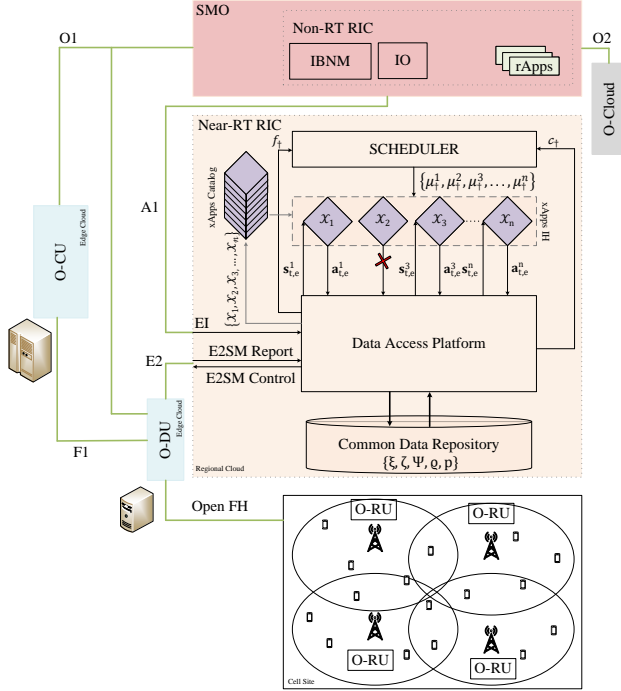


FIGURE 3: Proposed framework with workflow

enables operators to specify their intents using a high-level language through the Intent Interface [1], [9] and converts these high-level intents into the corresponding low-level configuration directives by leveraging large language model (LLM) schemes [62]–[66], aligning with existing SMO practices. The Non-RT RIC parses these intents to deploy the necessary set of rApps and xApps, while IO ensures that xApps and rApps fulfil operator intents and prevent conflicts from multiple applications managing the same KPMs or NCPs [67]. Furthermore, leveraging a global network perspective and access to external sources, the Non-RT RIC and SMO relay EI to the Near-RT RIC via the A1 [68]. EI enhances RAN performance by providing data typically unavailable to the RAN, such as capacity forecasts, external data, and aggregate analytics. For example, a rApp within the Non-RT RIC can supply the Near-RT RIC with EI on the predicted evolution of KPMs over the next few seconds for specific users.

B. Near-RT RIC

According to O-RAN specifications in [31], the Near-RT RIC incorporates a data access platform that manages data production, sharing, and access among xApps while functioning as middleware between the xApps and a shared data repository, thereby ensuring efficient data storage and distribution. The EI received via the A1 interface is also disseminated to relevant components, including the xApp catalog, to facilitate the deployment of selected xApps to the xApp inference host (IH). The E2 interface enables the Near-RT RIC and its xApps to collect relevant data (i.e.,

KPMs) from E2 nodes as E2SM reports for the near-real-time control of the RAN. Also, actions taken by xApps to update the NCPs delivered to RAN as E2SM control via E2 [69].

C. Scheduler

Upon receiving an intent from the MNO, the Non-RT RIC processes and selects appropriate xApps, $\{\mathcal{X}_1, \mathcal{X}_2, \dots, \mathcal{X}_n\}$, according to the target objective of intent, f , (e.g., maximizing data rate) and provides ε context variables, $c_\dagger = \{c_\dagger^1, c_\dagger^2, \dots, c_\dagger^\varepsilon\}$ as EI via A1 for each scheduling period \dagger . The scheduler is also modelled using the A2C algorithm, incorporating context variables c_\dagger and reward f_\dagger as inputs to determine the active xApps for the subsequent scheduling period. The scheduler sends an activation message, $\{\mu_\dagger^1, \mu_\dagger^2, \dots, \mu_\dagger^n \mid \mu_\dagger^n \in \{0, 1\}\}$, to xApps IH, thereby enabling the selected xApps to access the data repository and commence optimization based on their respective objectives. In other words, the *Actor* network for scheduler A2C model, $\pi_\theta(\mathbf{a}_\dagger \mid \mathbf{s}_\dagger)$, outputs a probability distribution over activation decisions, where the state vector $\mathbf{s}_\dagger = [c_\dagger^1, c_\dagger^2, \dots, c_\dagger^\varepsilon, f_\dagger]$ and the action vector $\mathbf{a}_\dagger = [\mu_\dagger^1, \mu_\dagger^2, \dots, \mu_\dagger^n]$.

V. PERFORMANCE EVALUATION

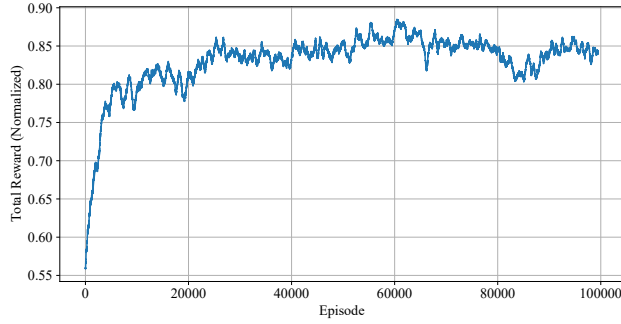
Table 1 presents the parameters of the simulation environment, which was created in Python to facilitate the training and testing of xApps and the scheduler, and which employs an O-RAN mobile network with four O-RUs concurrently serving 16 users.

A. Training of Power and RGB Allocation xApps

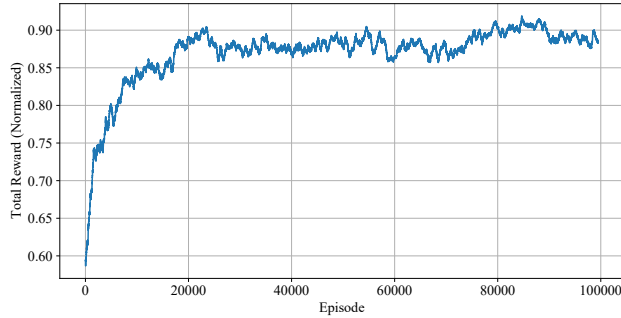
Training of the Power and RGB xApps is conducted in episodes, and the simulation environment is reset at the beginning of each episode ($t = 0$); the users are evenly distributed among four O-RUs, and each user $u \in U$ is randomly positioned at a distance between 150 and 450 m from their assigned O-RU. Both xApps are trained under the assumption of equal allocation of all other resources, which serves as a baseline allocation strategy. For instance, the available 12 RGBs for each O-RU are evenly distributed among connected users during the training of the Power xApp. For each episode e , the mean data arrival rate d_e and the average user speed, $\frac{1}{U} \sum_{u=1}^U v_e^u$, are randomly selected from the finite sets $\{3, 5, 7, 9\}$ Mbps and $\{10, 20, 30, 40\}$ m/s, respectively. The objective of both xApps is to maximize the normalized data transmission for each episode, τ_e , calculated as

$$\tau_e = \frac{\sum_{t=0}^{T-1} \tau_{t,e}}{d_e \times R \times B}, \quad \tau_{t,e} = \sum_{b=1}^B \sum_{r=1}^R \sum_{u=1}^U \delta_{t,e}^{b,r,u} \Psi_{t,e}^{b,r,u}, \quad (25)$$

where $\tau_{t,e}$ is the total data rate transmitted across all RBGs ($R \times B$) during each time step t in episode e and the maximum achievable data transmission is defined as the product of the average load d_e and the total number of



(a) Training of Power xApp



(b) Training of RGB xApp

FIGURE 4: Moving average reward of both xApps with a sliding window of 500

RBGs. The training results of the Power and RGB xApps are presented in Fig. 4, evaluated over 100,000 episodes, with each episode e comprising $\tilde{t} = 50$ time steps.

Fig. 5 illustrates the performance of the trained xApps—specifically, RBG-only, Power-only, and Both (i.e., when deployed independently)—across various scenarios defined by mean data arrival rates (low: 2 Mbps, mid: 5 Mbps, high: 8 Mbps) and average user speeds (low: 5 m/s, mid: 25 m/s, high: 45 m/s). Two primary observations can be drawn from the analysis. First, the independent control of parameters by concurrently deployed xApps, in the absence of coordination, leads to performance degradation across all scenarios. Second, the severity of these conflicts depends on network state variables; notably, performance degradation reaches 16% in the high scenario (8 Mbps, 45 m/s), compared to 5% in the low scenario (2 Mbps, 5 m/s). The conflicting behavior of these xApps can be attributed to their independent resource allocation actions. For example, conflicts may occur when the Power xApp assigns a specific power level to an RBG that is not allocated to any user by the RGB xApp. Conversely, conflicts may also arise when the RGB xApp assigns a substantial number of RBGs to a user, while the Power xApp provides a relatively low power allocation for those RBGs.

TABLE 1: Simulation Parameters

Parameter	Value / Description
Number of O-RUs (B)	4
Inter-site distance	900 m
Resource blocks (RBs)	100 RBs, each with 12 subcarriers
Resource block groups (RBGs) (R)	12 RBGs per O-RU
Carrier configuration	20 MHz bandwidth
Max transmission power (P_{min})	38 dBm
Min transmission power (P_{max})	1 dBm
Additive white Gaussian noise	-114 dBm
Propagation model	$120.9 + 37.6 \log(v)$ dB
Log-Normal shadowing	8 dB
Traffic model of arrival load (d_e)	{3, 5, 7, 9} Mbps
Number of users (U)	16
User speed range (v^u)	$V_{min} = 1$ m/s, $V_{max} = 50$ m/s
Probability of altering direction (ρ)	0.3
Training episodes	10^5
Time slots per episode (\tilde{t})	50
Scheduling period (\dagger)	10
Slot duration (T)	100 ms
Learning rate (η)	10^{-4}
Discount factor (γ)	0.95
α in (17)	0.5

B. Training of Scheduler

The initial condition for power and RGB allocation at the beginning of each episode is assumed to be an equal division, as established during the individual training of the xApps. Although the scheduler can be configured to optimize multiple objectives, this study specifically focuses on maximizing the normalized transmission rate achieved by both xApps. Additionally, the reward for the scheduler is computed on an episodic basis over $\dagger = 10$ time steps.

Method 1: Keep previous action

In this method, the training of the scheduler is carried out with two pre-trained A2C xApps—the power (\mathcal{X}_1) and RGB (\mathcal{X}_2)—to decide which xApp(s) to activate, choosing between individual or simultaneous deployment of these xApps. The scheduler is designed to make multiple decisions within a single episode (i.e., five decisions per episode ($\dagger = 10$ time steps)) and share these decisions through activation messages, $\mu_{\dagger} = \{\mu_{\dagger}^1, \mu_{\dagger}^2\}$ where $\mu_{\dagger}^n \in \{0, 1\} \quad \forall n = 1, 2$. Two context variables, $\{c_{\dagger}^1, c_{\dagger}^2\}$, representing the average user speed and mean data arrival rate are utilized as the state elements of the scheduler for each scheduling period \dagger during the training. This iterative approach enables the scheduler to refine its activation strategy continuously. Furthermore, if only one xApp is activated at a given decision interval, the system retains the last action made by the previously deactivated xApp, ensuring operational consistency throughout the training.

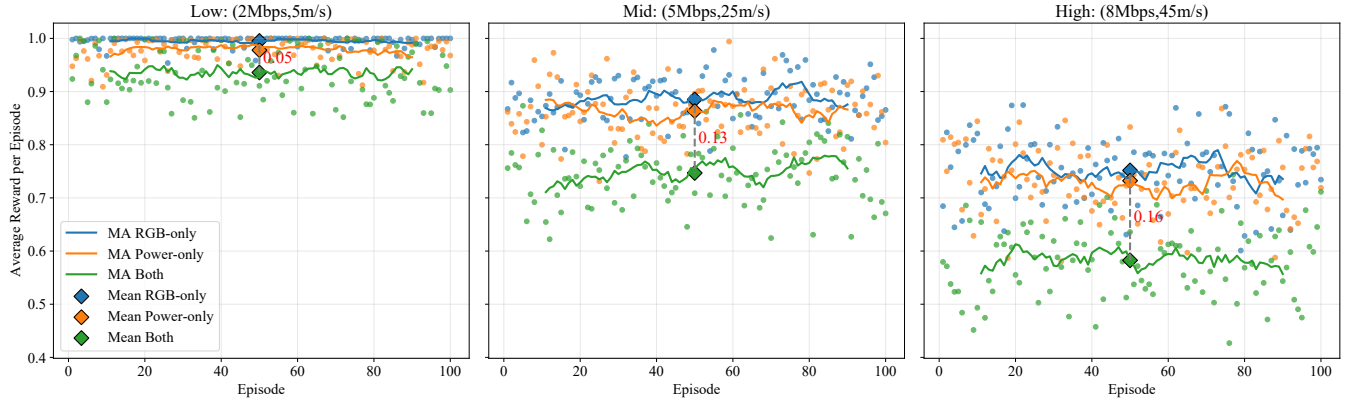


FIGURE 5: Performance comparison of trained xApps and conflicting case

Method 2: Extend with baselines

In this method, the scheduler training is conducted with two pre-trained A2C xApps—the power and RGB xApps—together with two baseline allocation xApps. The scheduler is designed to select one xApp for power allocation (A2C (\mathcal{X}_1) or baseline (\mathcal{X}_3)) and one xApp for resource allocation (A2C(\mathcal{X}_2) or baseline (\mathcal{X}_4)) to be deployed either independently or simultaneously for a given episode, allowing various combinations of baseline and pre-trained models to be activated. This is done by binary activation messages: $\mu_{\dagger} = \{\mu_{\dagger}^1, \mu_{\dagger}^2, \mu_{\dagger}^3, \mu_{\dagger}^4\}$ where $\mu_{\dagger}^n \in \{0, 1\} \quad \forall n = 1, \dots, 4$ subject to the constraints $\mu_{\dagger}^1 + \mu_{\dagger}^3 = 1$ and $\mu_{\dagger}^2 + \mu_{\dagger}^4 = 1$. Two context variables, $\{c_{\dagger}^1, c_{\dagger}^2\}$, representing the average user speed and mean data arrival rate are utilized as the state elements of the scheduler for each scheduling period \dagger during the training.

C. Simulation Results

It is assumed that an intent is received as: "maximize the total transmission rate across all O-RUs" and the Non-RT RIC selects xApps, $\{\mathcal{X}_1, \mathcal{X}_2, \mathcal{X}_3, \mathcal{X}_4\}$ based on target, f , of the total transmission rate defined in (25). This set of trained xApps is deployed to xApp IH to be managed by the scheduler.

Fig. 6 compares the performance of multiple active trained xApp variations, including *RGB-only*(\mathcal{X}_4), *Power-only* (\mathcal{X}_2), and *Both* ($(\mathcal{X}_2), (\mathcal{X}_4)$) deployed independently; *Both* ($(\mathcal{X}_2), (\mathcal{X}_4)$) with scheduler that considers only two A2C-trained xApps while retaining the last action from a deactivated xApp; and a *4 xApps* ($(\mathcal{X}_1), (\mathcal{X}_2), (\mathcal{X}_3), (\mathcal{X}_4)$) with scheduler scenario where the scheduler selects one xApp from each group of power and RGB allocations. These comparisons are conducted with context variables categorized into low,

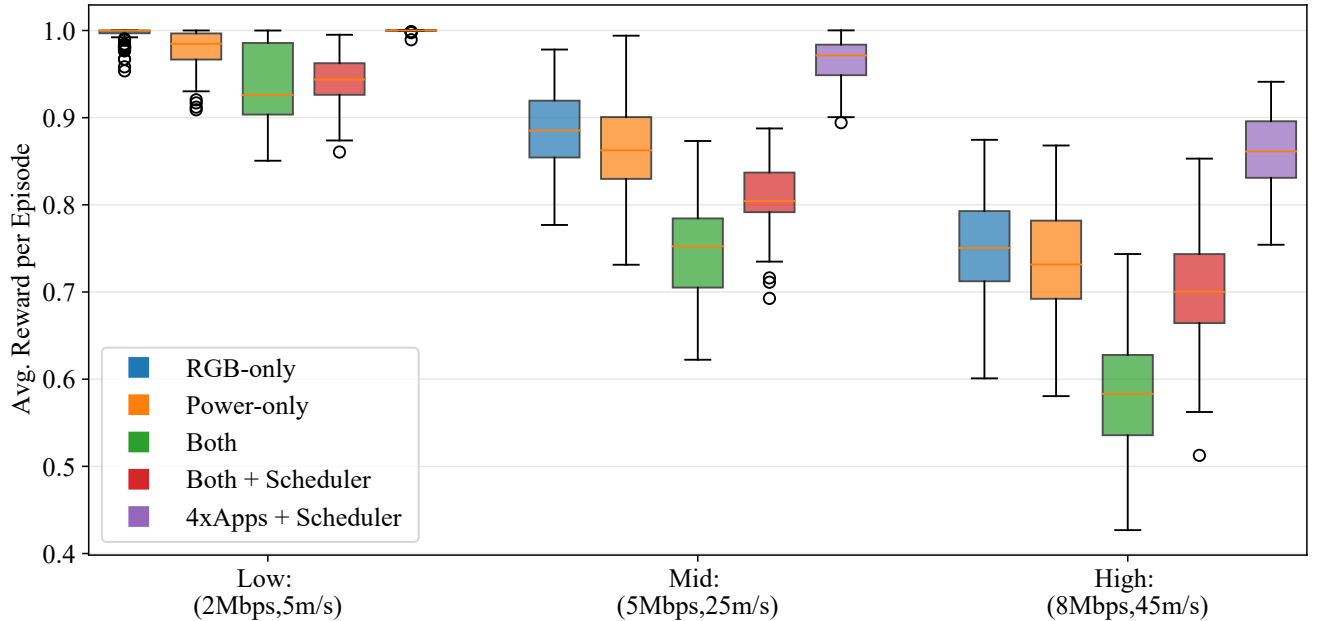


FIGURE 6: Performance comparison of xApps in the presence of a scheduler, based on the reward defined in (25).

mid, and high values. It can be observed that the scheduler utilizing both trained A2C xApps demonstrates improved performance compared to the conflicting case; however, its performance remains inferior to that achieved through individual deployment of the xApps. Extending the set of available xApps to include baseline xApps and permitting the scheduler to select from this expanded group yields the best results, surpassing even the performance of individual xApp deployments.

VI. CONCLUSION

In the O-RAN network considered here, multiple distributed O-RUs rely on xApps for essential tasks, such as power and resource block allocations. Despite its capacity for data-driven control, the O-RAN paradigm necessitates robust coordination among pre-trained xApps, as their actions can occasionally conflict. This work underscores the inherent challenges in estimating KPMs for diverse action combinations of active xApps in the absence of an accurate digital twin, and highlights the context-dependent nature of conflicts in automated network management. Recognizing that pre-trained and validated xApps cannot be modified post-deployment, this study introduces an intent-driven, scheduler-based conflict mitigation framework that selects active xApps based on contextual variables and target KPMs, without necessitating further xApp re-training. Through simulation of an indirect conflict scenario involving Power and RGB allocation xApps, and by leveraging the A2C method for training both the xApps and the scheduler, it is demonstrated that while a scheduler utilizing only A2C-trained xApps improves performance relative to independently deployed conflicting xApps, its performance is suboptimal compared to individual deployments. Notably, extending the available set of xApps to include baseline configurations and enabling the scheduler to choose from this expanded pool yielded the most favorable results. These findings advocate for further exploration into adaptive scheduling mechanisms and a broader xApp selection framework to enhance conflict resolution and ensure optimal network performance in dynamic, real-world deployments. The ideal scheduler should dynamically manipulate pre-trained xApps based on context-specific network state variables and be easily updated to accommodate various intents and combinations of xApps.

ACKNOWLEDGMENT

The authors would like to express their gratitude to Prof. Osvaldo Simeone for his significant contributions to the formulation of the solution presented in this work. Author Idris Cinnere is funded for his Ph.D. by the Ministry of National Education in Türkiye (2018). Also, this work was supported by the Open Fellowships of the EPSRC EP/W024101/1.

REFERENCES

- [1] Noe M Yungaicela-Naula, Vishal Sharma, and Sandra Scott-Hayward. Misconfiguration in o-ran: Analysis of the impact of ai/ml. *Computer Networks*, page 110455, 2024.
- [2] Joao F Santos, Alexandre Huff, Daniel Campos, Kleber V Cardoso, Cristiano B Both, and Luiz A DaSilva. Managing o-ran networks: xapp development from zero to hero. *arXiv preprint arXiv:2407.09619*, 2024.
- [3] Xingqin Lin, Lopamudra Kundu, Chris Dick, and Soma Velayutham. Embracing ai in 5g-advanced toward 6g: A joint 3gpp and o-ran perspective. *IEEE Communications Standards Magazine*, 7(4):76–83, 2023.
- [4] Michele Polese, Mischa Dohler, Falko Dressler, Melike Erol-Kantarci, Rittwik Jana, Raymond Knopp, and Tommaso Melodia. Empowering the 6g cellular architecture with open ran. *IEEE Journal on Selected Areas in Communications*, 2023.
- [5] ETSI. Ng-ran; architecture description, version 17.0.0. *3GPP Standard (TS) 38.401*, 2022.
- [6] Prabhu Kaliyammal Thiruvassagam, Vinay Venkataram, Vivek Raja Ilangovan, Maneesha Perapalla, Rajisha Payyanur, Vishal Kumar, et al. Open ran: Evolution of architecture, deployment aspects, and future directions. *arXiv preprint arXiv:2301.06713*, 2023.
- [7] Mohamad Wani, Mathias Kretschmer, Bernd Schröder, Andreas Grebe, and Michael Rademacher. Open ran: A concise overview. *IEEE Open Journal of the Communications Society*, 6:13–28, 2025.
- [8] Khurshid Alam, Mohammad Asif Habibi, Matthias Tammen, Dennis Krummacker, Walid Saad, Marco Di Renzo, Tommaso Melodia, Xavier Costa-Pérez, M erouane Debbah, Ashutosh Dutta, et al. A comprehensive overview and survey of o-ran: Exploring slicing-aware architecture, deployment options, and use cases. *arXiv preprint arXiv:2405.03555*, 2024.
- [9] Michele Polese, Leonardo Bonati, Salvatore D’Oro, Stefano Basagni, and Tommaso Melodia. Understanding o-ran: Architecture, interfaces, algorithms, security, and research challenges. *IEEE Communications Surveys & Tutorials*, 25(2):1376–1411, 2023.
- [10] Aly S. Abdalla, Pratheek S. Upadhyaya, Vijay K. Shah, and Vuk Marojevic. Toward next generation open radio access networks: What o-ran can and cannot do! *IEEE Network*, 36(6):206–213, 2022.
- [11] Anil Umesh Tatsuro Yajima, Toru Uchino, and Suguru Okuyama. Overview of o-ran fronthaul specifications. *NTT DOCOMO Technical Journal*, 21(1), 2019.
- [12] Mojdeh Karbalaee Motalleb, Vahid Shah-Mansouri, and Salar Nouri Naghadeh. Joint power allocation and network slicing in an open ran system. *arXiv preprint arXiv:1911.01904*, 2019.
- [13] Line MP Larsen, Henrik L Christiansen, Sarah Ruepp, and Michael S Berger. The evolution of mobile network operations: A comprehensive analysis of open ran adoption. *Computer Networks*, page 110292, 2024.
- [14] Bouziane Brik, Karim Boutiba, and Adlen Ksentini. Deep learning for b5g open radio access network: Evolution, survey, case studies, and challenges. *IEEE Open Journal of the Communications Society*, 3:228–250, 2022.
- [15] Amath Ndao, Xavier Lagrange, Nicolas Huin, Geraldine Texier, and Loutfi Nuaymi. Optimal placement of virtualized dnn in o-ran architecture. In *2023 IEEE 97th Vehicular Technology Conference (VTC2023-Spring)*, pages 1–6. IEEE, 2023.
- [16] Wilfrid Azariah, Fransiscus Asisi Bimo, Chih-Wei Lin, Ray-Guang Cheng, Navid Nikaiein, and Rittwik Jana. A survey on open radio access networks: Challenges, research directions, and open source approaches. *Sensors*, 24(3):1038, 2024.
- [17] Andres Garcia-Saavedra and Xavier Costa-P erez. O-ran: Disrupting the virtualized ran ecosystem. *IEEE Communications Standards Magazine*, 5(4):96–103, 2021.
- [18] Roger Niklasson, Rajavarma Bhyrraju, Kedar Thakar, David Espadas, Gustavo Hylander, and Justin Paul. An intelligent platform: The use of o-ran’s smo as the enabler for openness and innovation in the ran domain. White Paper BDGS-21:031169, Ericsson, 2021.
- [19] ORAN Alliance. O-ran work group 1 (use cases and overall architecture) o-ran architecture description. *O-RAN.WG1.OAD-R003-v12.00 Technical Specification*, 2024.
- [20] Leonardo Bonati, Michele Polese, Salvatore D’Oro, Stefano Basagni, and Tommaso Melodia. Open, programmable, and virtualized 5g networks: State-of-the-art and the road ahead. *Computer Networks*, 182:107516, 2020.
- [21] Simona Marinova and Alberto Leon-Garcia. Intelligent o-ran beyond 5g: Architecture, use cases, challenges, and opportunities. *IEEE Access*, 12:27088–27114, 2024.

- [22] Federico Mungari. An rl approach for radio resource management in the o-ran architecture. In *2021 18th Annual IEEE International Conference on Sensing, Communication, and Networking (SECON)*, pages 1–2, 2021.
- [23] Rawlings Ntassah, Gian Michele Dell’Aera, and Fabrizio Granelli. xapp for traffic steering and load balancing in the o-ran architecture. In *ICC 2023 - IEEE International Conference on Communications*, pages 5259–5264, 2023.
- [24] Han Zhang, Hao Zhou, and Melike Erol-Kantarci. Federated deep reinforcement learning for resource allocation in o-ran slicing. In *GLOBECOM 2022-2022 IEEE Global Communications Conference*, pages 958–963. IEEE, 2022.
- [25] Leonardo Bonati, Salvatore D’Oro, Michele Polese, Stefano Basagni, and Tommaso Melodia. Intelligence and learning in o-ran for data-driven nextg cellular networks. *IEEE Communications Magazine*, 59(10):21–27, 2021.
- [26] Hanchao Yang, Connor Mcpeak, Rakesh Nagampally, Nishith Tripathi, Gustave Anderson, Jeffrey H. Reed, Yaling Yang, and Daniel J. Jakubisin. Agile 5g networks: Advance traffic steering xapp for interference mitigation. In *MILCOM 2024 - 2024 IEEE Military Communications Conference (MILCOM)*, pages 300–305, 2024.
- [27] Mahdi Eskandari, Shipra Kapoor, Keith Briggs, Arman Shojaeifard, Huiling Zhu, and Alain Mourad. Smart interference management xapp using deep reinforcement learning. *arXiv preprint arXiv:2204.09707*, 2022.
- [28] Chujie Wang, Zhifeng Zhao, Qi Sun, and Honggang Zhang. Deep learning-based intelligent dual connectivity for mobility management in dense network. In *2018 IEEE 88th Vehicular Technology Conference (VTC-Fall)*, pages 1–5, 2018.
- [29] Oner Orhan, Vasuki Narasimha Swamy, Thomas Tetzlaff, Marcel Nassar, Hosein Nikopour, and Shilpa Talwar. Connection management xapp for o-ran ric: A graph neural network and reinforcement learning approach. In *2021 20th IEEE international conference on machine learning and applications (ICMLA)*, pages 936–941. IEEE, 2021.
- [30] Andrea Lacava, Michele Polese, Rajarajan Sivaraj, Rahul Soundraran, Bhawani Shanker Bhati, Tarunjeet Singh, Tommaso Zugno, Francesca Cuomo, and Tommaso Melodia. Programmable and customized intelligence for traffic steering in 5g networks using open ran architectures. *IEEE Transactions on Mobile Computing*, 23(4):2882–2897, 2023.
- [31] ORAN Alliance. O-ran working group 2:“o-ran ai/ml workflow description and requirements 1.03. *O-RAN.WG2.AIML-v01.03 Technical Specification*, 2021.
- [32] ORAN Alliance. O-ran working group 3:“(near-real-time ran intelligent controller and e2 interface) near-rt ric architecture”. *O-RAN.WG3.RICARCH-R003-v05.00 Technical Specification*, 2023.
- [33] ORAN Alliance. O-ran working group 3:“(near-real-time ran intelligent controller and e2 interface) conflict mitigation”. *O-RAN.WG3.TR.ConMit-R004-v01.00 Technical Specification*, 2024.
- [34] Cezary Adamczyk and Adrian Kliks. Conflict mitigation framework and conflict detection in o-ran near-rt ric. *IEEE Communications Magazine*, 61(12):199–205, 2023.
- [35] Cezary Adamczyk and Adrian Kliks. Detection and mitigation of indirect conflicts between xapps in open radio access networks. In *IEEE INFOCOM 2023 - IEEE Conference on Computer Communications Workshops (INFOCOM WKSHPs)*, pages 1–2, 2023.
- [36] Anastasios Giannopoulos, Sotirios Spantideas, Levis George, Kalafatis Alexandros, and Panagiotis Trakadas. Comix: Generalized conflict management in o-ran xapps—architecture, workflow, and a power control case. *arXiv preprint arXiv:2501.14619*, 2025.
- [37] Pietro Brach del Prever, Salvatore D’Oro, Leonardo Bonati, Michele Polese, Maria Tsampazi, Heiko Lehmann, and Tommaso Melodia. Pacifista: Conflict evaluation and management in open ran. *arXiv preprint arXiv:2405.04395*, 2024.
- [38] Abdul Wadud, Fatemeh Golpayegani, and Nima Afraz. Qacm: Qos-aware xapp conflict mitigation in open ran. *arXiv preprint arXiv:2405.07324*, 2024.
- [39] Abdul Wadud, Fatemeh Golpayegani, and Nima Afraz. Conflict management in the near-rt-ric of open ran: A game theoretic approach. *arXiv preprint arXiv:2311.13389*, 2023.
- [40] Han Zhang, Hao Zhou, and Melike Erol-Kantarci. Team learning-based resource allocation for open radio access network (o-ran). In *ICC 2022 - IEEE International Conference on Communications*, pages 4938–4943, 2022.
- [41] Pedro Enrique Iturria-Rivera, Han Zhang, Hao Zhou, Shahram Mollahasani, and Melike Erol-Kantarci. Multi-agent team learning in virtualized open radio access networks (o-ran). *Sensors*, 22(14):5375, 2022.
- [42] Hakan Erdol, Xiaoyang Wang, Robert Piechocki, George Oikonomou, and Arjun Parekh. xapp distillation: Ai-based conflict mitigation in b5g o-ran. *arXiv preprint arXiv:2407.03068*, 2024.
- [43] AB 3GPP. Nr; physical layer procedures for data. *3rd Generation Partnership Project (3GPP), Technical Specification (TS) 38.214*, 9, 2018.
- [44] Youngwoo Oh, Arif Ullah, and Wooyeol Choi. Multi-objective reinforcement learning for power allocation in massive mimo networks: A solution to spectral and energy trade-offs. *IEEE Access*, 12:1172–1188, 2024.
- [45] Fan Meng, Peng Chen, and Lenan Wu. Power allocation in multi-user cellular networks with deep q learning approach. In *ICC 2019 - 2019 IEEE International Conference on Communications (ICC)*, pages 1–6, 2019.
- [46] Ronald J Williams. Simple statistical gradient-following algorithms for connectionist reinforcement learning. *Machine learning*, 8:229–256, 1992.
- [47] Kevin Murphy. Reinforcement learning: An overview. *arXiv preprint arXiv:2412.05265*, 2024.
- [48] Richard S Sutton. Reinforcement learning: An introduction. *A Bradford Book*, 2018.
- [49] Thomas Degris, Patrick M Pilarski, and Richard S Sutton. Model-free reinforcement learning with continuous action in practice. In *2012 American control conference (ACC)*, pages 2177–2182. IEEE, 2012.
- [50] Vijay Konda and John Tsitsiklis. Actor-critic algorithms. *Advances in neural information processing systems*, 12, 1999.
- [51] Volodymyr Mnih. Asynchronous methods for deep reinforcement learning. *arXiv preprint arXiv:1602.01783*, 2016.
- [52] Yasar Sinan Nasir and Dongning Guo. Multi-agent deep reinforcement learning for dynamic power allocation in wireless networks. *IEEE Journal on Selected Areas in Communications*, 37(10):2239–2250, 2019.
- [53] Kazi Ishfaq Ahmed and Ekram Hossain. A deep q-learning method for downlink power allocation in multi-cell networks. *arXiv preprint arXiv:1904.13032*, 2019.
- [54] Yi Yang, Fenglei Li, Xinzhe Zhang, Zhixin Liu, and Kit Yan Chan. Dynamic power allocation in cellular network based on multi-agent double deep reinforcement learning. *Computer Networks*, 217:109342, 2022.
- [55] Shaomin Zhang, Lixin Li, Jiaying Yin, Wei Liang, Xu Li, Wei Chen, and Zhu Han. A dynamic power allocation scheme in power-domain noma using actor-critic reinforcement learning. In *2018 IEEE/CIC International Conference on Communications in China (ICCC)*, pages 719–723, 2018.
- [56] Mostafa Rahmani, Manijeh Bashar, Mohammad J. Dehghani, Pei Xiao, Rahim Tafazolli, and M erouane Debbah. Deep reinforcement learning-based power allocation in uplink cell-free massive mimo. In *2022 IEEE Wireless Communications and Networking Conference (WCNC)*, pages 459–464, 2022.
- [57] Lirui Luo, Jiayi Zhang, Shuaifei Chen, Xiaodan Zhang, Bo Ai, and Derrick Wing Kwan Ng. Downlink power control for cell-free massive mimo with deep reinforcement learning. *IEEE Transactions on Vehicular Technology*, 71(6):6772–6777, 2022.
- [58] Mohammed MH Qazzaz, Łukasz Kulacz, Adrian Kliks, Syed A Zaidi, Marcin Dryjanski, and Des McLernon. Machine learning-based xapp for dynamic resource allocation in o-ran networks. *arXiv preprint arXiv:2401.07643*, 2024.
- [59] Vaishnavi Kasuluru, Luis Blanco, and Engin Zeydan. On the use of probabilistic forecasting for network analysis in open ran. In *2023 IEEE International Mediterranean Conference on Communications and Networking (MeditCom)*, pages 258–263, 2023.
- [60] Claudio Fiandrino, Leonardo Bonati, Salvatore D’Oro, Michele Polese, Tommaso Melodia, and Joerg Widmer. Explora: Ai/ml explainability for the open ran. *Proceedings of the ACM on Networking*, 1(CoNEXT3):1–26, 2023.
- [61] Shahram Mollahasani, Melike Erol-Kantarci, and Rodney Wilson. Dynamic cu-du selection for resource allocation in o-ran using actor-critic learning. In *2021 IEEE Global Communications Conference (GLOBECOM)*, pages 1–6. IEEE, 2021.

- [62] Abdelkader Mkrache, Adlen Ksentini, and Christos Verikoukis. Intent-based management of next-generation networks: an llm-centric approach. *IEEE Network*, 38(5):29–36, 2024.
- [63] Nguyen Tu, Sukhyun Nam, and James Won-Ki Hong. Intent-based network configuration using large language models. *International Journal of Network Management*, 35(1):e2313, 2025.
- [64] Dimitrios Brodimas, Kostis Trantzas, Besiana Agko, Georgios Christos Tziavas, Christos Tranoris, Spyros Denazis, and Alexios Birbas. Towards intent-based network management for the 6g system adopting multimodal generative ai. In *2024 Joint European Conference on Networks and Communications and 6G Summit (EuCNC/6G Summit)*, pages 848–853, 2024.
- [65] Ahlam Fuad, Azza H. Ahmed, Michael A. Riegler, and Tarik Čičić. An intent-based networks framework based on large language models. In *2024 IEEE 10th International Conference on Network Softwarization (NetSoft)*, pages 7–12, 2024.
- [66] Joseph Mcnamara, Daniel Camps-Mur, Meysam Goodarzi, Hilary Frank, Lorena Chinchilla-Romero, Ferrán Cañellas, Adriana Fernández-Fernández, and Shuangyi Yan. Nlp powered intent based network management for private 5g networks. *IEEE Access*, 11:36642–36657, 2023.
- [67] Jingwen Zhang, Chungang Yang, Ru Dong, Yao Wang, Alagan Anpalagan, Qiang Ni, and Mohsen Guizani. Intent-driven closed-loop control and management framework for 6g open ran. *IEEE Internet of Things Journal*, 11(4):6314–6327, 2024.
- [68] ORAN Alliance. O-ran working group 2:“ai interface: General aspects and principles 2.03. *ORAN-WG2.AI.GAPv02.03 Technical Specification*, 2021.
- [69] Anastasios Giannopoulos, Sotirios Spantideas, Levis George, Kalafatis Alexandros, and Panagiotis Trakadas. Comix: Generalized conflict management in o-ran xapps – architecture, workflow, and a power control case, 2025.